Kinematic (mass) effects in reactions of the type *H+HL→HH+L*

Cite as: J. Chem. Phys. **76**, 4513 (1982); https://doi.org/10.1063/1.443576
Published Online: 31 August 1998

Augustin Siegel, and Arnulf Schultz

Kinematic (mass) effects in reactions in the type $H+HL \rightarrow HH+L$

Augustin Siegel[a] and Arnulf Schultz[b]

Fakultät für Physik, University of Freiburg, D 7800 Freiburg/Br., West Germany
(Received 7 April 1981; accepted 19 May 1981)

To get a better understanding of reactions such as Ba + HCl→BaCl + H 3*D* trajectory calculations of the type **H**→**HL**→**HH** + **L** (**H** = heavy, **L** = light) were performed on a number of different model potentials, at different collision energies. The study was mainly devoted to a systematic search for kinematic effects caused by the special mass combination. In (**H**→**HL**) reactions, kinematics play a dominant role in the reaction probability and in the impact parameter dependence of the product molecule energies. It is therefore possible to draw further information from direct experimental results. All kinematic effects found can be simply explained by the relatively small moment of inertia of the light particle. Some insight into the dynamics of such reactions is also obtained.

INTRODUCTION

In a previous article we reported on the determination of the product state distribution for the reactions Ba + HX → BaX + H (X = Cl and Br) as a function of the collision energy.[1] Like many alkali-atom hydrogen halide reactions these two reactions possess a very pronounced mass balance of the type **H** + **HL** → **HH** + **L** (**H** = heavy, **L** = light). Application of the conservation laws to thermoneutral (**H** + **HL**) reactions show the existence of a very efficient transfer of the angular momentum L of the reactants to the angular momentum J' of the product molecules. Examples are the reactions K + HBr or Cs + HBr.[2] Trajectory calculations indicate that the relation $J' \simeq L$ may hold also for exothermic reactions like Ba + HX, even at high collision energies.[3,4]

In addition to the angular momenta, there may be other quantities in (**H** + **HL**) reactions which are correlated to each other by the special mass ratio. It is very important to know all these relationships in order to be sure which experimentally determined quantities provide information on the reaction dynamics (potential surface), and which quantities just reflect the special kinematics (mass ratios). The qualitative understanding of the reactive process may also be improved considerably, if one understands the kinematics. In order to find out these kinematical relationships we carried out trajectory calculations on model potentials for the general triatomic reaction A + BC → AB + C. In Ref. 1 we already used the results described below for an analysis of our experimental results for the reactions Ba + HCl and Ba + HBr.

This work was actually stimulated by the question of whether additional information about the potential surfaces of (**H** + **HL**) systems could be obtained if vibrational population distributions are measured at various collision energies. A simple impulsive model shows that the appearance of large product vibration must be related to small impact parameters, and vice versa. We demonstrate in this article that the vibrational population distribution changes substantially with both the potential surface and the collision energy. The rotational distribution, on the other hand, is found to be essentially determined by the kinematics, i.e., not much can be learned about the dynamics of (**H** + **HL**) reactions by a measurement of the rotational energy distribution.

CALCULATION PROCEDURE

The program used for the trajectory calculations was originally written by D. L. Bunker. The integration procedure was changed from a Runge–Kutta method to a Hamming predictor–corrector method with variable integration step size.

The model surfaces are of the LEPS (see, for example, Ref. 5) and hyperbolic map function (HMF) types.[6,7] These two types of model potentials differ enough to ensure that none of the effects found is due to the analytical form of the surfaces. Table I summarizes the parameters of the four basic surfaces used for the calculations. We also made some additional calculations for thermoneutral and endothermic reac-

TABLE I. Surface parameters.

(a) Morse parameters common for all surfaces

D_{AB} = 4.24 eV	r_{AB} = 2.72 Å	β_{AB} = 0.9109 Å^{-1}
D_{BC} = 4.436 eV	r_{BC} = 1.274 Å	β_{BC} = 1.898 Å^{-1}
D_{AC} = 1.82 eV	r_{AC} = 2.2318 Å	β_{AC} = 1.112 Å^{-1}

(b) Other surface parameters

	κ_{AB}	κ_{BC}	κ_{AC}
LEPS1	0.15	0.08	0.15
LEPS2	0.15	0.20	0.15

	u_0	v_0	a	A	n
HMF1[a]	0.12	−0.5	1.5	4	3
HMF2[a]	0.40	−0.5	1.5	4	3

[a]The meaning of the HMF parameters can be found in Ref. 7. Eqs. (1)–(9).

[a]Present address: Fachbereich Physik, University of Kaiserslautern, D 6750 Kaiserslautern, West Germany.

[b]Present address: Uranit GmbH, D 5170 Jülich, West Germany.

 0021-9606/82/094513-15$02.10

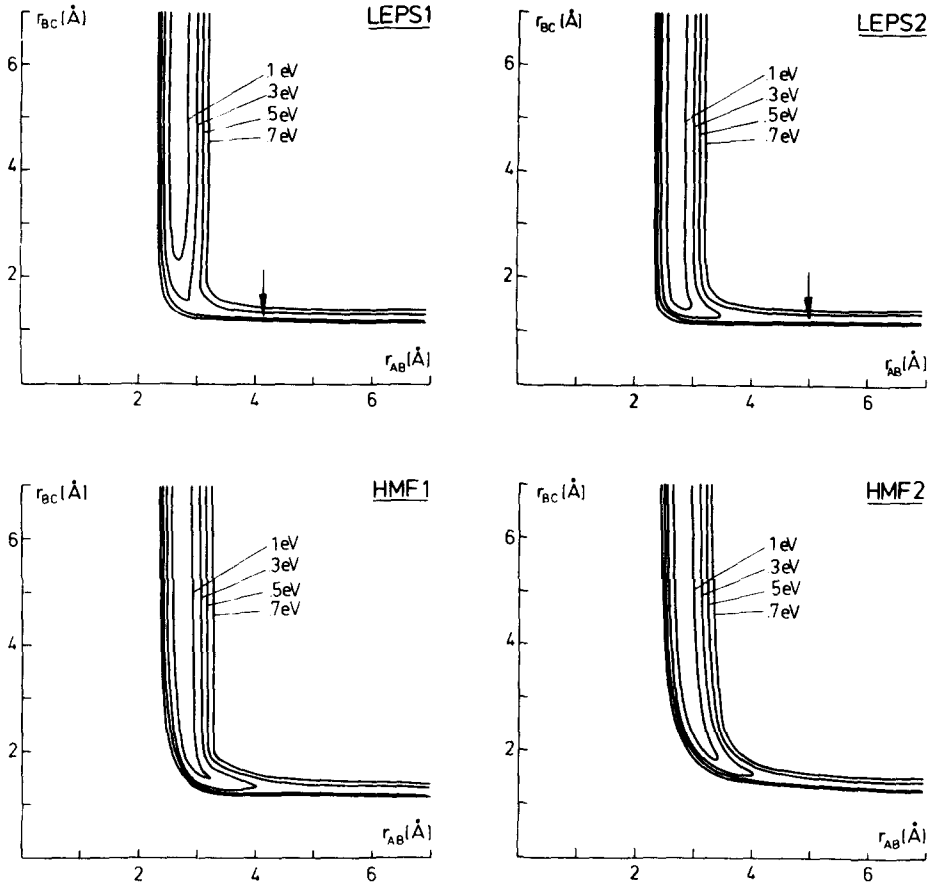

FIG. 1. Collinear cuts through the basic potential hypersurfaces used in the trajectory calculations. Arrows indicate the location of small barriers (~0.03 eV) on the LEPS surfaces.

tions. For this purpose, surfaces were derived from the basic ones by changing the value of the dissociation energy D_{AB}. No surface with a basin in the potential was used.

The Morse parameters of the diatomic potentials are those of the molecules BaCl, HCl, and BaH, common for both the LEPS and the HMF surfaces. Figure 1 shows collinear cuts of the four surfaces. The LEPS surfaces exhibit small barriers (~0.03 eV) in the entrance valley. The location of these barriers is indicated by arrows in Fig. 1. The two LEPS surfaces differ mainly in the region of the energy release. LEPS1 is of the late downhill type, whereas LEPS2 belongs to the early downhill type. Both HMF surfaces show early downhill character. HMF1 and HMF2 differ in the bend of the minimum energy path as projected onto the (r_{AB}, r_{BC}) plane. The bend is sharper for surface HMF1 than for HMF2. For the LEPS surfaces this bend is always rather sharp as a consequence of their analytical form.

The mass combinations used in the calculations are listed in Table II. Masses are given in amu throughout this article. m_A, m_B, and $m_C = 137$, 35, and 1 are the masses of Ba, Cl, and H. This mass combination represents our extreme case of **H + HL**. With the masses m_A, m_B, and $m_C = 137, 35$, and 4, the sensitivity of the kinematic effects to mass changes is tested. For the two additional mass combinations m_A, m_B, and $m_C = 137$, 18, and 18, and 137, 1, and 35, the mass balances differ from **H + HL** with the result that all kinematic effects typical for **H+HL** vanish almost completely. For the mass combination m_A, m_B, and $m_C = 137$, 1, and 35, only a small percentage of the trajectories turned out to be reactive. Therefore no results will be shown for this mass combination. However, the kinematic effects vanish to the same extent as in the examples given for m_A, m_B, and $m_C = 137$, 18, and 18.

The initial conditions are chosen to be close to those of our experiments.[1] Since we used a supersonic nozzle beam the vibrational and rotational energy of the reagent molecules E_{vib} and E_{rot} are set to zero. Even without the use of a nozzle beam this would be a good approximation for hydrogen halides as reagent molecules. Some calculations were done with $E_{vib} \neq 0$. These calculations are very time consuming because the very fast oscillations of the hydrogen halides determine the upper limit of the integration step size. The collision

TABLE II. Mass combinations in amu.

m_A	m_B	m_C
137	35	1
137	35	4
137	18	18
137	1	35

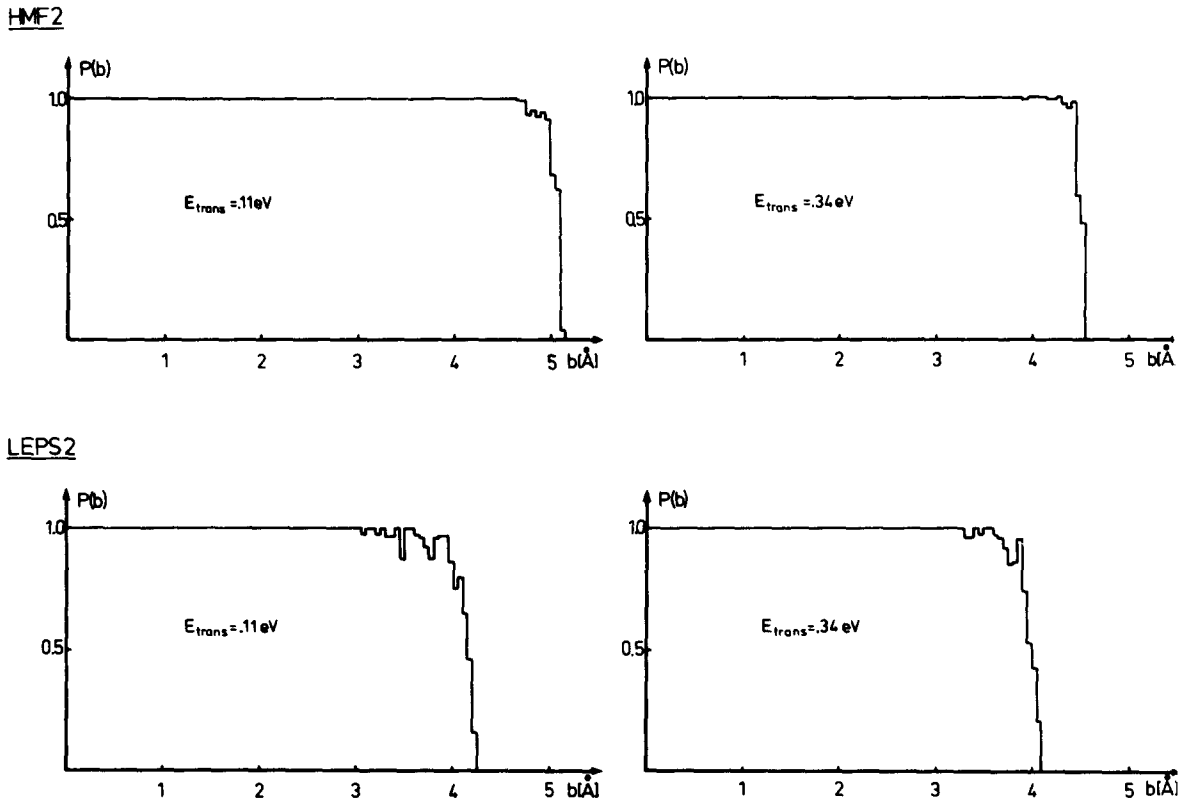

FIG. 2. Histograms of the reaction probability $P(b)$ for several surfaces and the mass combination m_A, m_B, and $m_C = 137$, 35, and 1. Step size in the histograms is 0.05 Å. 30–50 trajectories are calculated per histogram unit.

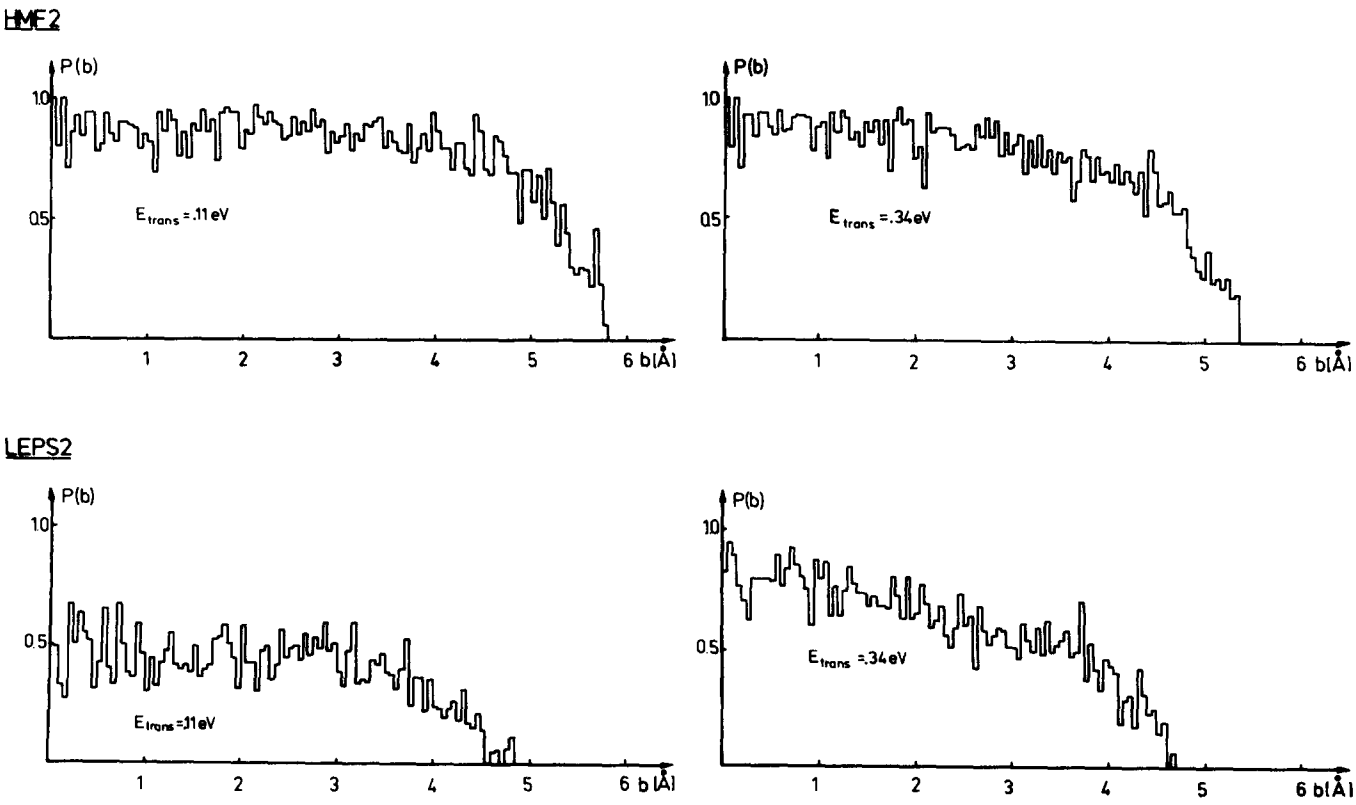

FIG. 3. Histograms of the reaction probability $P(b)$ for the masses m_A, m_B, and $m_C = 137$, 18, and 18.

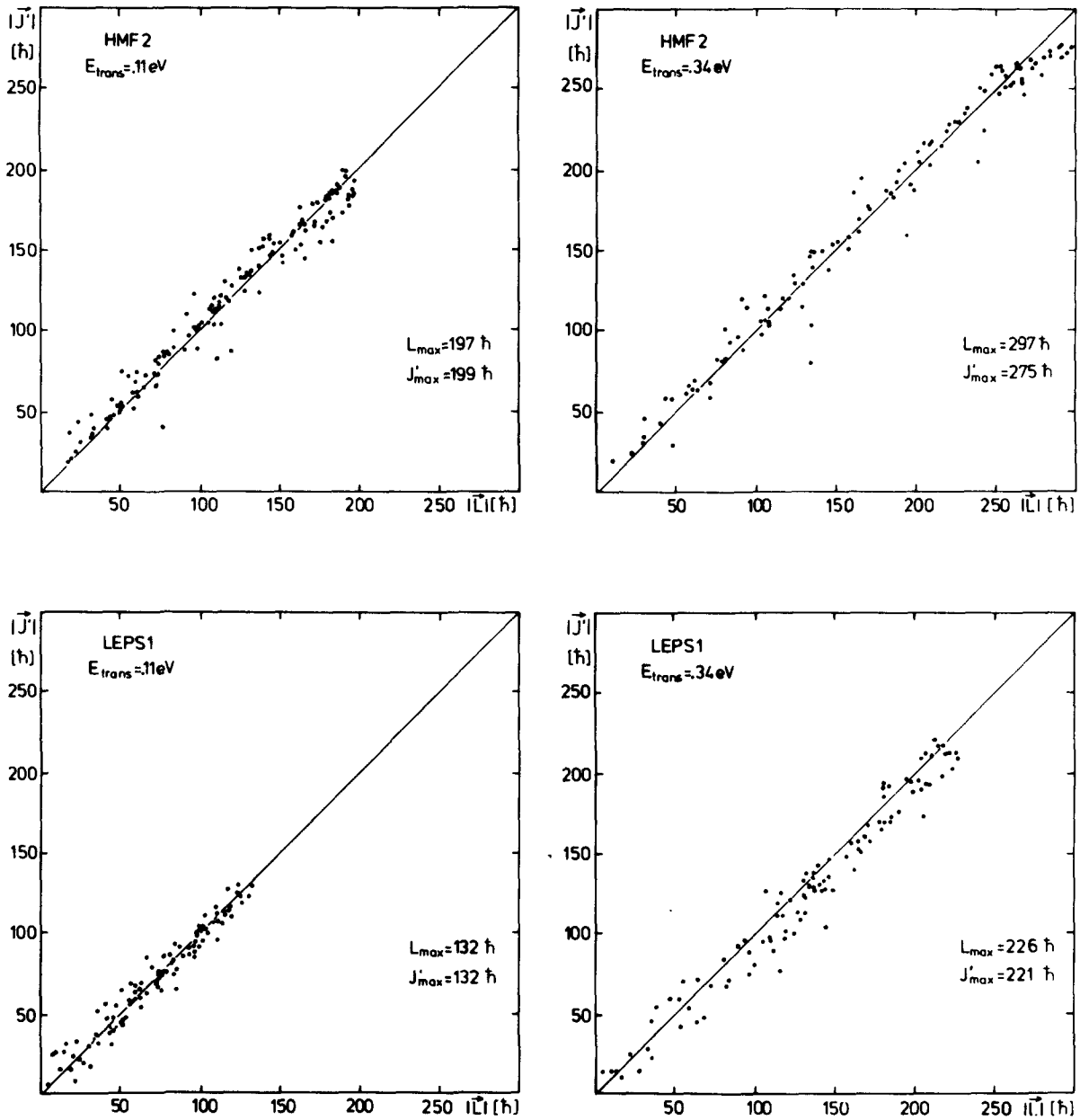

FIG. 4. Correlation of J' and L for the mass combination m_A, m_B, and $m_C = 137$, 35, and 1 for two surfaces and two collision energies. Every point represents the result of a single trajectory.

energy is set to the fixed values 0.11 and 0.34 eV according to our two experimental boundary values. The remaining initial conditions—impact parameter and initial position of the three atoms—are chosen statistically by a Monte Carlo method.

RESULTS

In order to find kinematic effects, the results of many single trajectories were surveyed with the goal of finding functional dependences and correlations between the different quantities. Since it is impossible to show results for all the surfaces by figures, only typical examples are shown. For all the other surfaces the results look quite the same as far as the kinematical effects are concerned.

We found three different kinematic effects:

(1) The reaction probability $P(b)$ as a function of the impact parameter b is a step function of the form

$$P(b) = \begin{cases} 1 \text{ for } b \leqq b_{\max} \\ 0 \text{ for } b > b_{\max} \end{cases} , \quad (1)$$

Figure 2 shows calculated histograms of the function $P(b)$. The step size in the histograms is $b = 0.05$ Å. About 30–50 trajectories are calculated per histogram unit. The masses of the three atoms in these calculations are m_A, m_B, and $m_C = 137$, 35, and 1. The examples shown belong to two different model surfaces, and to two different collision energies.

Almost all collisions for small impact parameters in

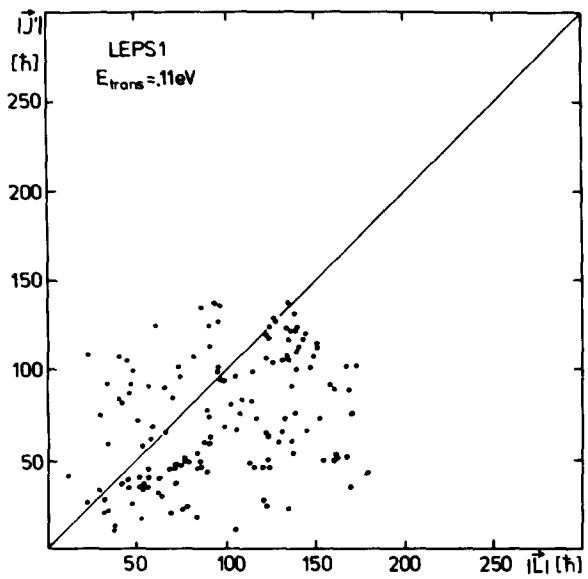

FIG. 5. J' as a function of L for the mass combination m_A, m_B, and $m_C = 137$, 18, and 18.

these examples lead to reaction irrespective of the surface and the collision energy. The reaction probability sharply drops to zero within a small region of impact parameters. The value of b_{max} depends on both the surface and the collision energy. The same behavior for the function $P(b)$ is observed for all other surfaces as long as the masses are m_A, m_B, and $m_C = 137$, 35, and 1. The drop of the reaction probability from one to zero always takes place within a few tenths of an angstrom. So the step function character of the function $P(b)$ is a very good approximation for all our surfaces, at least for all collision energies within the range chosen in the present calculations.

If the masses are changed to m_A, m_B, and $m_C = 137$, 18, and 18 the shape of $P(b)$ changes drastically and becomes dependent on both the surface and the collision energy, as is shown in Fig. 3. The surfaces and collision energies are the same as in Fig. 2. Strong steric effects hindering the reaction at small impact parameters show up. Note that b_{max} is somewhat different from the values observed for the previous mass combination.

In the function $P(b)$, b_{max} only depends on the surface and the collision energy for **H + HL**. The mechanisms determining b_{max} for the surfaces used here are discussed below.

(2) The rotational angular momentum of the product molecules J' is to a very good approximation equal to the orbital angular momentum of the reactants

$$J' \simeq L .$$

The close correlation of these two quantities is demonstrated in Fig. 4. Every point represents the result of a single reactive trajectory. For this presentation the density of points was chosen to be essentially constant within each interval Δb. Since the initial angular momentum of the reagent molecule is zero, L is equal to the total angular momentum. Therefore the deviations of the points in Fig. 4 from the straight line $J' = L$ indicate the value of the product angular momentum L'. For all surfaces used in the calculations the percentage of trajectories with $L' > 20\hbar$ was less than 10%.

If the masses are changed again to m_A, m_B, and $m_C = 137$, 18, and 18 the correlation between J' and L becomes very weak as can be seen in Fig. 5 as an example.

The result of $J' = L$ is in agreement with results obtained by Polanyi *et al.*[3,4] on different surfaces and at different collision energies. So, for the extreme cases of the mass combination **H + HL** the angular momentum of the product molecule J' is almost exclusively determined by kinematics. Since L_{max}, the maximal angular momentum for which reaction is observed, is a function of the potential surface as well as of the collision energy, J'_{max} is also dependent on these quantities.

(3) There exists a strong correlation between the product vibrational energy E'_{vib} and the impact parameter as well as between the product translational energy E'_{trans} and the impact parameter.

In Fig. 6 the product vibrational and translational energies are plotted as a function of the impact parameter for the masses m_A, m_B, and $m_C = 137$, 35, and 1. As before, every point is the result of a single trajectory. The correlation between E'_{vib} and b on the one side and E'_{trans} and b on the other side is apparent. Figure 6(c) shows an example of a calculation where the BC molecule is vibrationally excited by 0.2 eV. This differs from other calculations of this work. The correlation remains, and the average value of E'_{vib} (b) at a given impact parameter b increases by just the same amount of additional initial vibrational energy. The correlation effects disappear, however, almost completely if one changes the masses again to m_A, m_B, and $m_C = 137$, 18, and 18. This is shown in Fig. 7.

Note, however, that the impact parameter dependence of the mean energies $\bar{E}'_{vib}(b)$ and $\bar{E}'_{trans}(b)$ [the bar stands for the average value of $E'_{vib}(b)$ and $E'_{trans}(b)$ at a given impact parameter b] is certainly *not* determined by the mass ratio; instead it is given by the potential surface and by the initial conditions (E_{trans}, E_{vib}, E_{rot}) as can be seen in Fig. 6. Therefore, the population distribution of the vibrational and translational product states must depend on these quantities. Since measurements of the vibrational population distributions N_v were performed by us,[1] it is interesting to know the sensitivity of N_v to the potential surfaces as well as to the collision energy. Figure 8 presents some results of these calculations. The shape of N_v changes quite substantially with both the surfaces and the collision energy. The present calculations were not done, however, with the intention of finding—by a systematic variation of potential parameters—a surface which fits the experimental N_v data best. So far there is at most a qualitative agreement between the experimental and calculated distributions N_v.

DISCUSSION

The following discussion is intended to provide a qualitative understanding for the existence of the kinema-

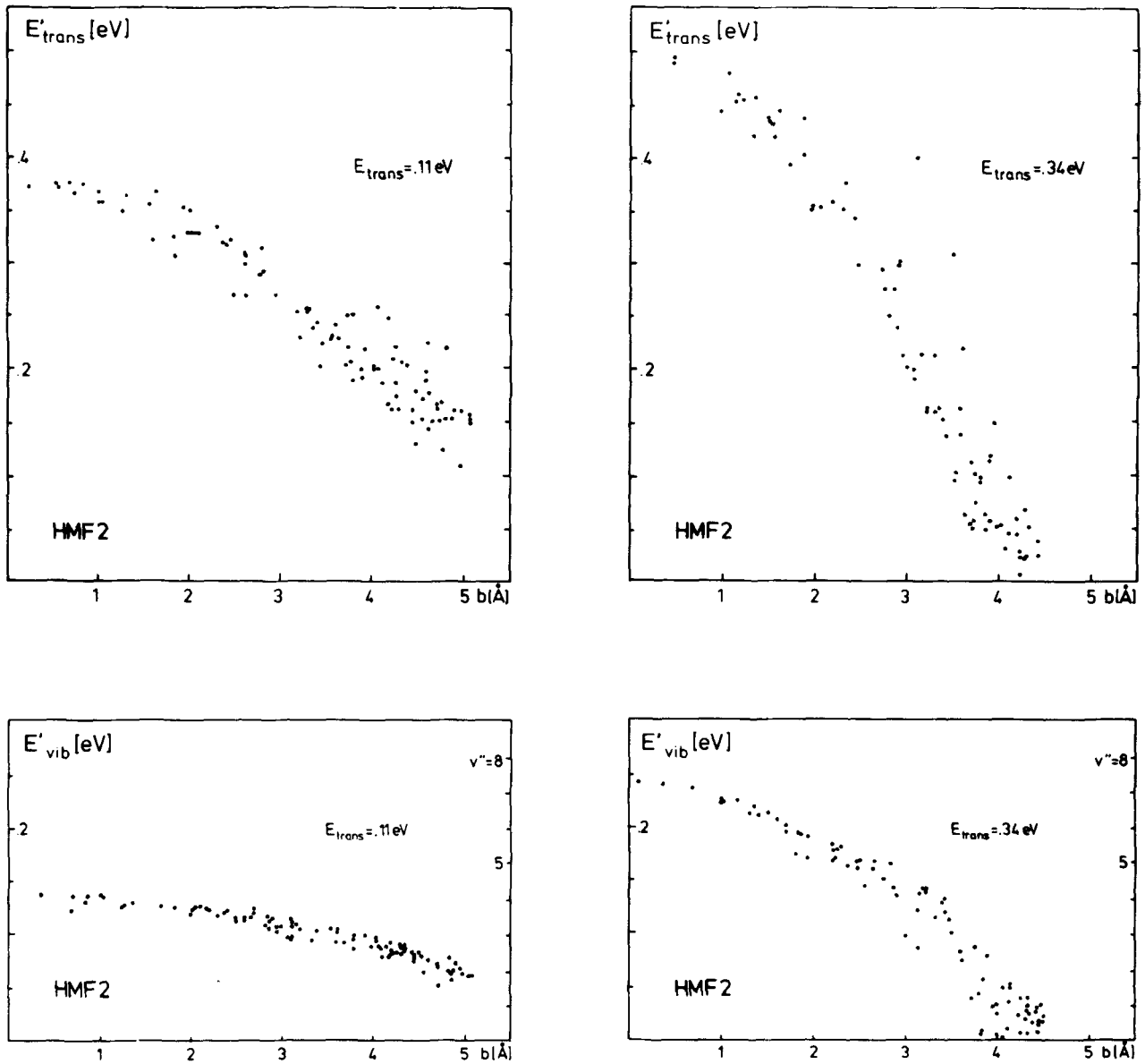

FIG. 6. Correlation of product energies E'_{vib} and E'_{trans} with the impact parameter b for the masses m_A, m_B, and $m_C = 137$, 35, and 1. For the construction of the parabolic curves in the upper part of (b) see the text. While all the other calculations presented in this article refer to BC molecules without initial vibrational rotational energy, part (c) shows a result with BC molecules of 0.2 eV initial vibrational energy.

FIG. 6. (*Continued*).

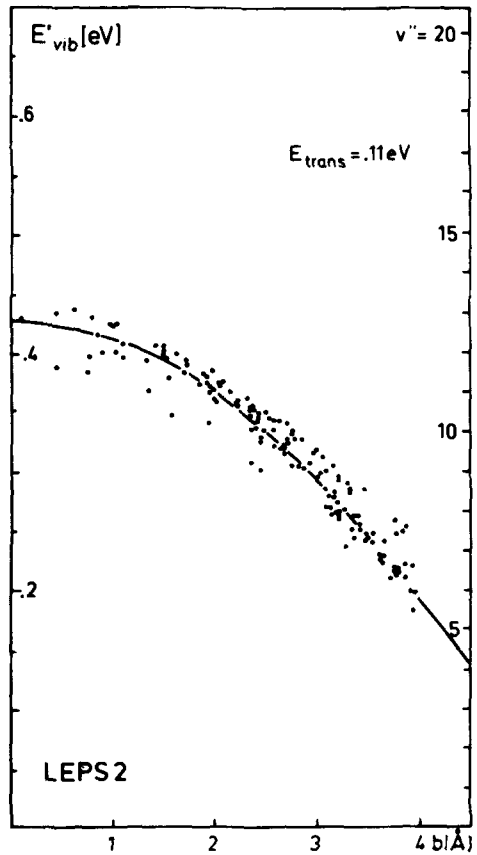

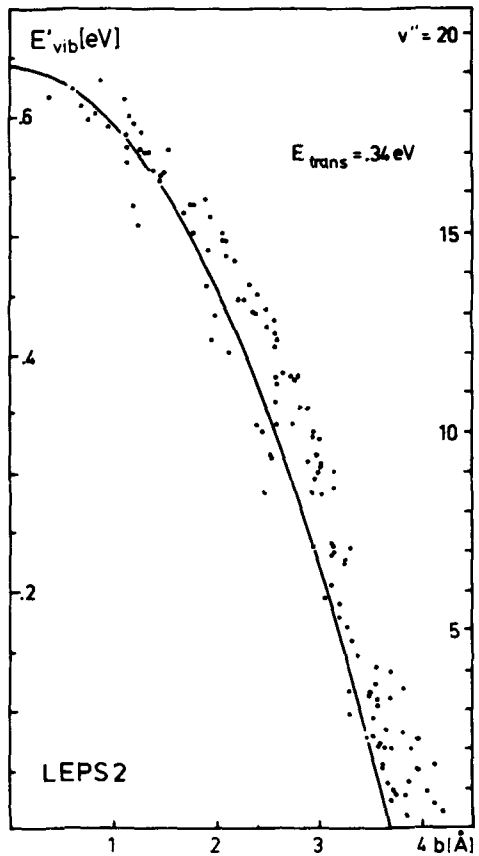

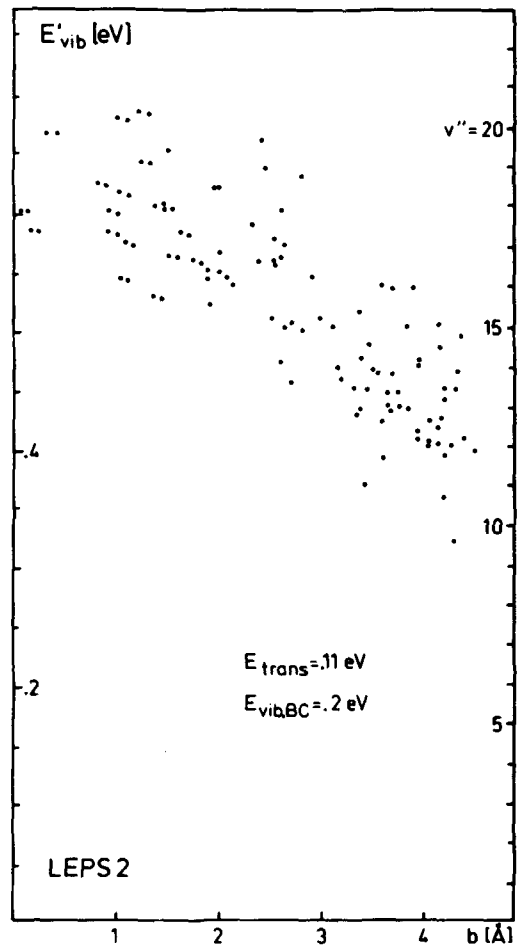

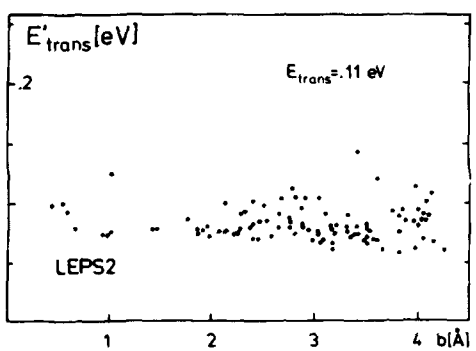

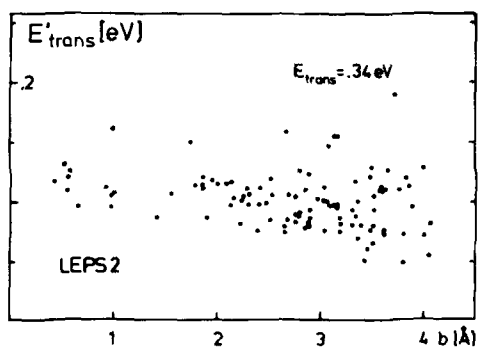

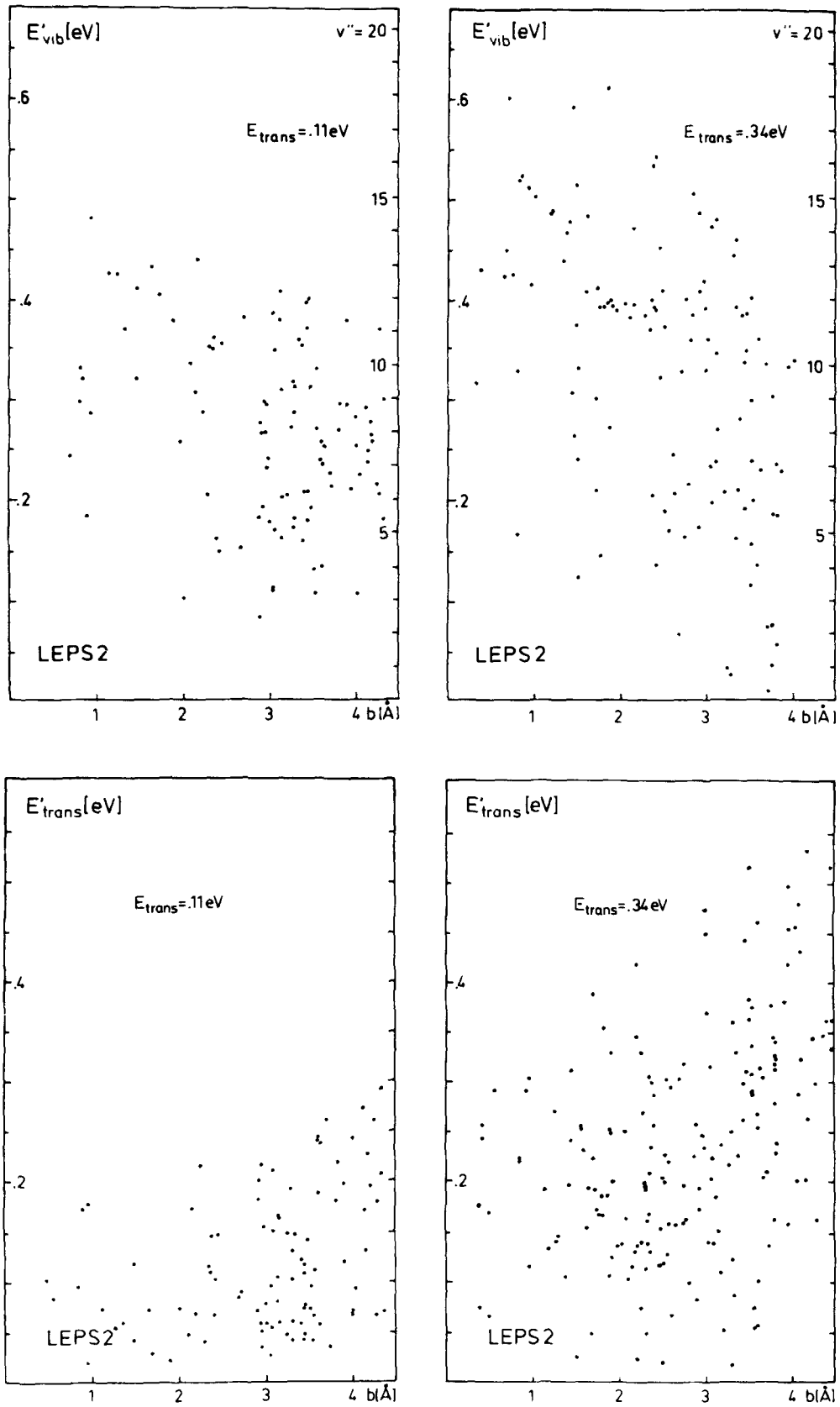

FIG. 7. E'_{vib} and E'_{trans} as functions of the impact parameter b for the masses m_A, m_B, and $m_C = 137$, 18, and 18 for surface LEPS2.

tic peculiarities just described. As a second topic it will be shown how these peculiarities can be used to draw additional information from experimentally determined quantities such as mean product rotational energies or vibrational population distributions.

Qualitative understanding of the kinematics

The reason for the existence of the kinematic effects is the very small mass of the atom C in comparison to the masses m_A and m_B or, in other words, the

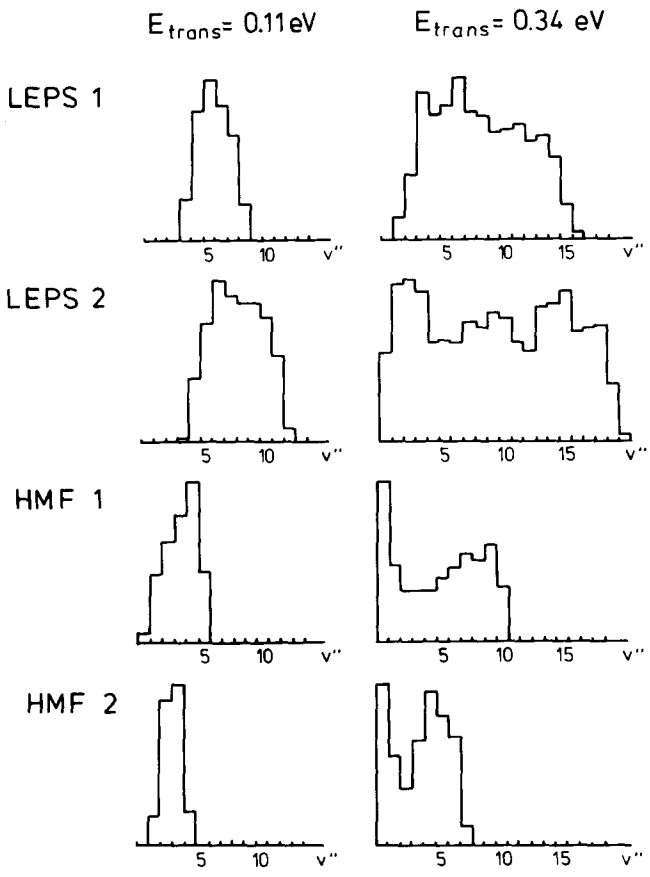

FIG. 8. Histograms of vibrational population distributions. For an explanation of the appearance of bimodal distributions for the HMF surfaces at $E_{trans}=0.34$ eV see the text.

very small moment of inertia I_{BC} of the molecule BC compared to those of the systmes A–B and A–BC with BC treated as one particle.

This point will be discussed now for the three effects separately and illustrated by some typical trajectories, which are shown in Fig. 9. In this figure the paths of the three atoms are drawn as a function of time. Time is marked along the paths in units of 10^{-14} s. The calculations for these trajectories were done on surface LEPS2 at a collision energy 0.5 eV and for the masses m_A, m_B, and $m_C=137$, 35, and 1. The initial vibrational and rotational energy was zero as before. As a consequence of an appropriate choice of the initial momenta the three atoms stay in a plane during the reaction. They exhibit, however, the essential characteristics of out of plane trajectories also.

To explain the special shape of the function $P(b)$ one has to find out why there are practically no nonreactive collisions for small impact parameters and what causes the sharp drop in the reaction probability at b_{max}. Nonreactive collisions at small impact parameters are mainly caused by steric hindering of the reaction. Figure 9(a) now shows a trajectory with impact parameter $b=0$ and with initial positions of the three atoms very close to the collinear configuration A–C–B. With these conditions, steric effects in general will hinder reaction strongly. Steric hindering indeed plays some role in the collision shown in Fig. 9(a). The time marks along the path of atom B indicate a decrease of the relative velocity of the atoms A and B. This decrease is caused by the repulsion acting between the atoms A and C. This repulsion is strongest in the linear configuration A–C–B. Due to the very small momentum of inertia I_{BC} the system approaches the minimum energy configuration, i.e., the opposite linear configuration A–B–C, very fast and starts an oscillatory motion around it. In this way the effect of steric hindering is much smaller than it would be in cases of a larger moment of inertia I_{BC}. Our trajectory calculations have shown that for the masses m_A, m_B, and $m_C=137$, 35, and 1, reaction would not take place if the angle $\sphericalangle$(ABC) is half the angle in Fig. 9(a) or less. A few cases of steric hindering of the reaction can even be found in the range of impact parameters $0<b<b_{max}$, if one adjusts the initial conditions in a proper way. However, all these cases of hindering possess an estimated statistical weight of less than 1% for all surfaces used here.

In a similar way one can understand the sharp drop in the reaction probability at b_{max} and the mechanisms determining the cross section. As long as the bond of the molecule BC exists, a two particle approximation with BC treated as one particle will describe the system very well. This is because the momentum of atom C as well as the angular moment of BC stay small compared to the total momentum and the total angular momentum, respectively.. With this two particle approximation an angular momentum barrier can be calculated, and it turns out that in many cases the barrier determines the value of b_{max}. This can be seen, for example, in Fig. 10(a) for surface HMF2 at the collision energy 0.11 eV. In Fig. 10(a) the effective potential along the minimum energy path is drawn for $b_{max}=5.15$ Å as given by the trajectory calculations. The barrier gives a strict upper limit for impact parameters of reactive collisions. This is true because the angular momentum J of BC remains small during the approach of the reagents and therefore the orbital angular momentum L stays constant to a very good approximation until the bond BC is broken.

In Fig. 10(b) the effective potential of HMF2 is drawn in the same manner as for the collision energy 0.34 eV. The value $b_{max}=4.55$ Å, which is observed in the calculations, was used to determine the effective potential. One can see that in this case the barrier top is well below the energy 0.34 eV, i.e., the angular momentum barrier does not completely determine the cross section. Using $J'=L$ to calculate the product rotational energy for $b_{max}=4.55$ Å, it turns out that the total energy of the reaction is contained in product rotation. In this case the cross section is determined then by conservation of angular momentum $J'=L$, valid for our mass combination. The upper limit for the impact parameters of reactive collisions is very strict again, because L is constant as before.

The change in the mechanism determining the cross section is observed for all HMF surfaces used in our calculations, because the minimum energy paths of these

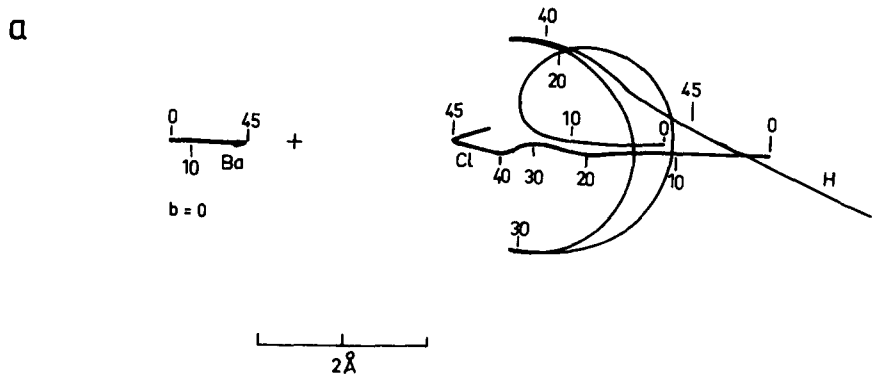

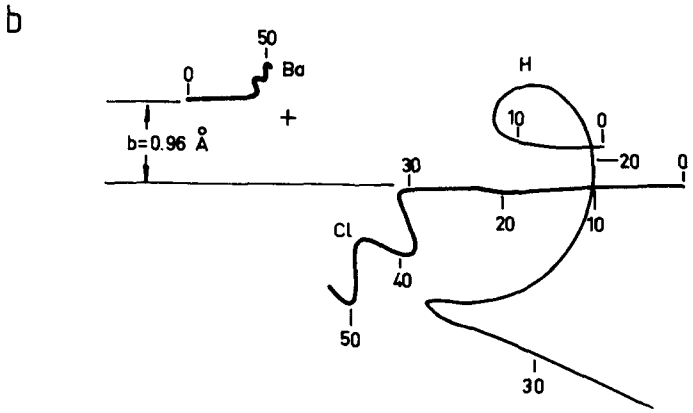

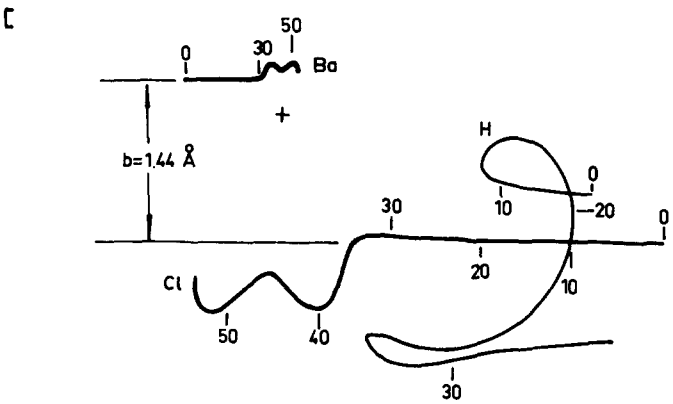

FIG. 9. Single trajectories calculated on surface LEPS2. $E = 0.5$ eV. Time is marked along the paths of the three atoms in units of 10^{-14} s. The cross indicates the center of mass.

surfaces are very similar. For the LEPS surfaces used here the cross section is determined by the angular momentum barrier in any case.

Indications to the change of this mechanism can be seen at least in two instances of the results of our calculations: (1) small, but significant deviations of the points from the straight line $J' = L$ can be seen in Fig. 4 (surface HMF2, collision energy 0.34 eV) for the largest L values. The same is observed for the other HMF surfaces. (2) The vibrational population distribution of the HMF surfaces shows a qualitative change in going from the collision energy 0.11 to 0.34 eV (Fig. 8). At the higher collision energy a second peak appears at $v = 0$ in the distribution. This second peak corresponds to collisions with impact parameters close to b_{max}, i.e., the total energy of the reaction is almost completely contained in product rotation.

The explanation for the existence of the two remaining kinematic effects follows again from the small momentum of inertia I_{BC}. To point this out, it is convenient to express the correlation between J' and L as a correlation between the rotational energy of the product

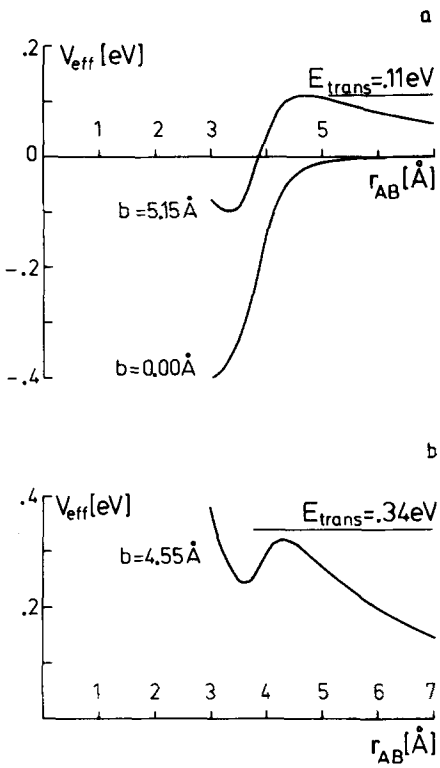

FIG. 10. Effective potentials along the minimum energy path for surface HMF2 calculated in a two particle approximation for $b = 0$ Å and b_{max} observed in the calculations for the energies 0.11 and 0.34 eV.

molecule AB and the impact parameter:

$$E'_{rot}(b) = J'^2/2\mu_{AB}r_{AB}^{02} \simeq L^2/2\mu_{AB}r_{AB}^{02} = (\mu_{A,BC}vb)^2/2\mu_{AB}r_{AB}^{02} \simeq E_{trans}(b/r_{AB}^0)^2 , \quad (2)$$

where μ is the reduced mass, v the initial relative velocity, and r_{AB}^0 the equilibrium distance of the molecule AB. Therefore, both effects can be described as correlations between product energies and the impact parameter.

The quantities of our initial conditions, which are chosen statistically, are the impact parameter and the orientation of BC with respect to A. Therefore the existence of a strong correlation between product energies and the impact parameter indicates that the product energies are, to a very large extent, independent of the initial orientation of BC. This independence is caused again by the small momentum of inertia I_{BC}. As long as the bond of BC exists, this small momentum of inertia enables the system to approach the minimum of the potential energy irrespective of the initial orientation. Qualitatively this can be seen in the Figs. 9(b) and 9(c). Two trajectories with different impact parameters are drawn there. Both trajectories show again the fast motion of atom C. Reaction takes place in a much shorter time than in the trajectory shown in Fig. 9(a) (i. e., after approximately 30 time units, rather than 45), because steric hindering plays no role here. Therefore the motion of atom C does not show a

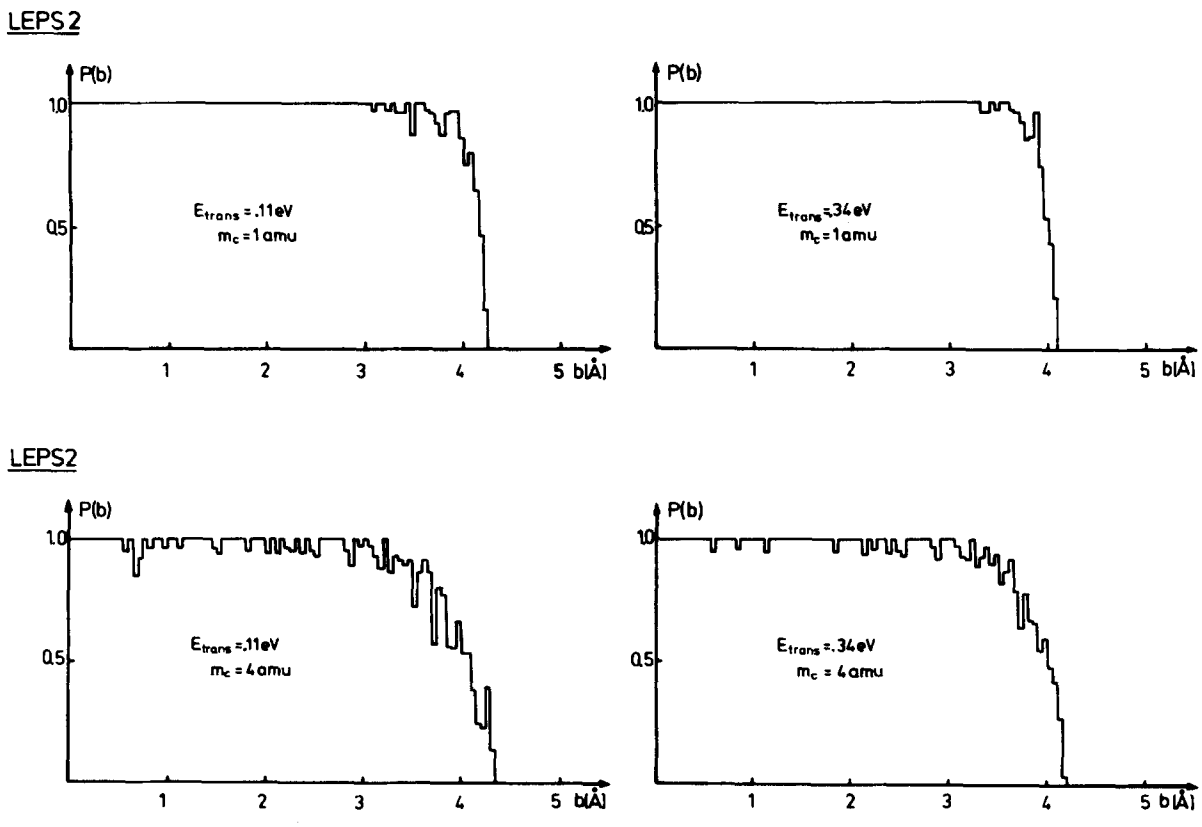

FIG. 11. Change in the reaction probability function in going from $m_C = 1$ (top) to $m_C = 4$ (bottom).

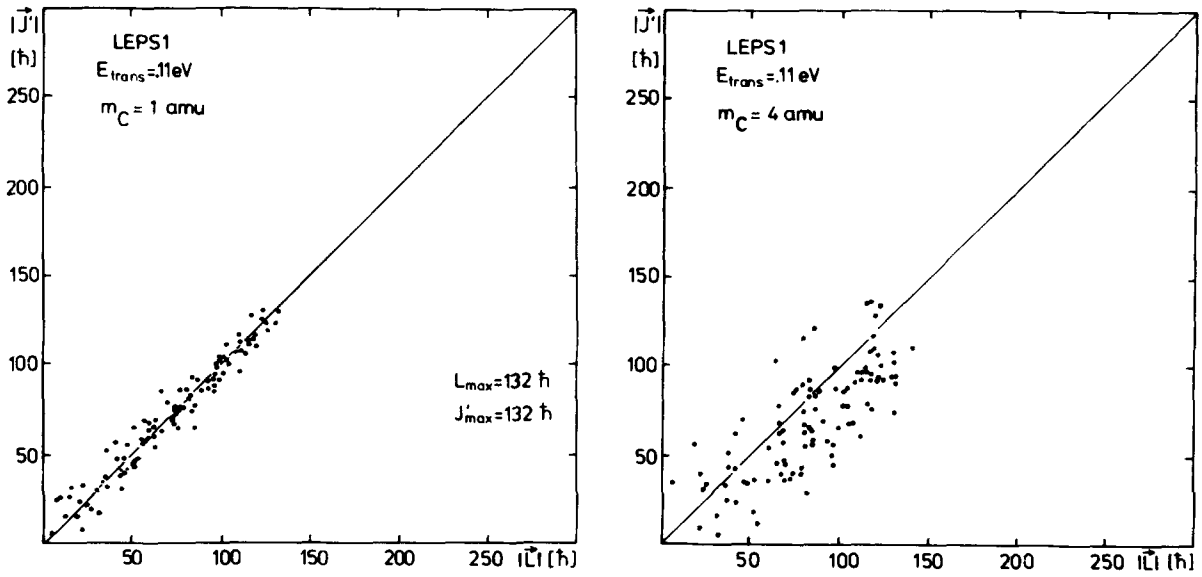

FIG. 12. Comparison of the correlation of J' and L for $m_C = 1$ (left) and $m_C = 4$ (right).

full oscillation, but only half a cycle. Note that atom C is out of the range of the figure long before the atoms A and B reach the ends of the paths which are drawn. Following the paths of A and B after reaction has taken place, one can see the vibrational rotational motion of the product molecule AB. If one takes the vibrational period as the time unit, one can see that an increased impact parameter yields an increased rotational energy of AB.

By conservation of energy $E_{tot} = \bar{E}'_{vib}(b) + \bar{E}'_{trans}(b) + \bar{E}'_{rot}(b)$. For the LEPS calculations it turned out that $\bar{E}'_{trans}(b)$ is nearly independent of b. With a constant value $\bar{E}'_{trans}(b)$ taken from the lower part of Fig. 6(b) and with $\bar{E}'_{rot}(b)$ determined by Eq. (2), $\bar{E}'_{vib}(b)$ becomes a parabolic function as is shown in the upper part of Fig. 6(b). In the same way the curves $\bar{E}'_{vib}(b)$ were constructed in Fig. 13.

The kinematic effects are very pronounced if the masses m_A, m_B, and $m_C = 137$, 35, and 1 are used in the calculations. In order to see, at least qualitatively, how sensitive the kinematic effects react on changes of the moment of inertia I_{BC}, we did some calculations with the masses m_A, m_B, and $m_C = 137$, 35, and 4. This corresponds to an increase of I_{BC} by a factor of 3.7. Results of these calculations are shown in Figs. 11–13 in comparison to results obtained with $m_C = 1$. In all the examples shown the kinematic effects become weaker in the case of $m_C = 4$ compared to the results with $m_C = 1$.

Additional information from experimental results

In experiments described in Ref. 1, we determined the vibrational population distribution N_v and the mean product energies of the BaX molecules formed in the reaction Ba + HX → BaX + H (X = Cl and Br) at various collision energies. Since the kinematic effects are very pronounced in these cases, they can be used to establish relations between measured quantities and other quantities of interest. This will be shown now by a few examples.

Absolute reaction cross section $\sigma_{re}(E_{trans})$

The mean rotational energy is defined as

$$\bar{E}'_{rot}(E_{trans}) = \int_0^{b_{max}} f(b) E'_{rot}(b)\, db \,, \tag{3}$$

with the partition function of the impact parameters given by

$$f(b) = 2b/b^2_{max} \tag{4}$$

if $P(b)$ is a step function as in Eq. (1). With Eq. (2) and with the approximation $\mu_{AB} \simeq \mu_{A,BC}$ one obtains by integration of Eq. (3)

$$\bar{E}'_{rot}(E_{trans}) = E_{trans} b^2_{max}/2r^{0^2}_{AB} \equiv E_{trans}\sigma_{re}(E_{trans})/2\pi r^{0^2}_{AB} \,. \tag{5}$$

Equation (5) allows us to determine the absolute cross section from the mean product rotational energy. In Ref. 1 we have presented reactive cross sections derived in this way for the reaction Ba + HX → BaX + H (X = Cl and Br).

In a similar way Toennies *et al.* [8] have determined the cross section of the reaction Rb + HBr. In their experiment the mean rotational energy was measured using an electrostatic quadrupole state selector. They assumed $P(b)$ was a step function in their determination.

Detailed vibrational cross sections $\sigma_{re}(E_{trans}, v)$

With $\sigma_{re}(E_{trans})$ as derived above, detailed vibrational cross sections $\sigma_{re}(E_{trans}, v)$ were determined in Ref. 1 from the experimental vibrational population distributions N_v as

$$\sigma_{re}(E_{trans}, v) = \sigma_{re}(E_{trans}) N_v \,. \tag{6}$$

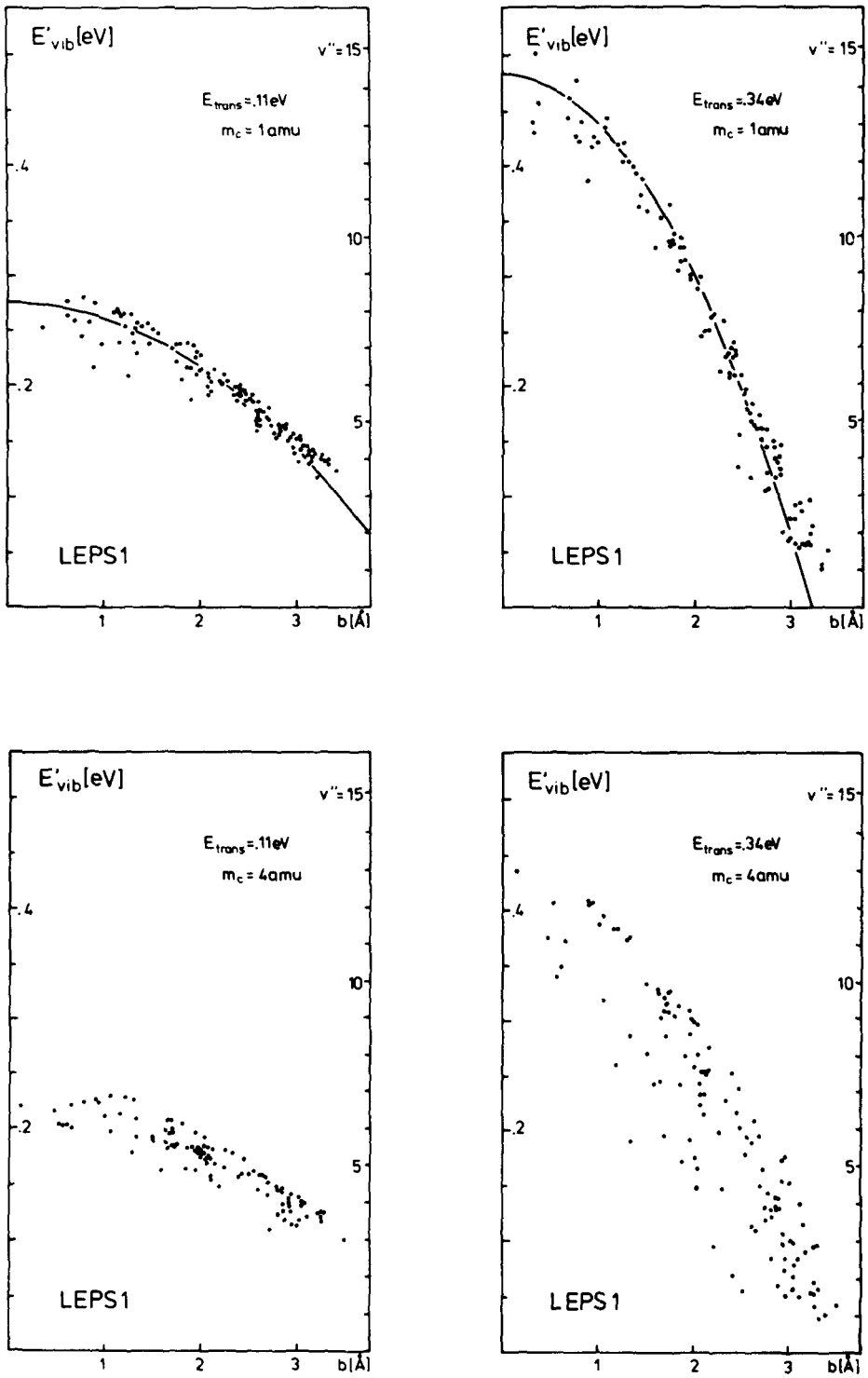

FIG. 13. Change in the correlation between E'_{vib} and b in going from $m_C = 1$ (top) to $m_C = 4$ (bottom). For the construction of the parabolic curve in the upper part of the figure see the text.

The function v(b)

With the knowledge about the strong correlation between the product vibrational energy and the impact parameter the cross section $\sigma_{re}(E_{trans}, v)$ can be expressed by

$$\sigma_{re}(E_{trans}, v) = 2\pi \int_{b(v+1)}^{b(v)} b' P(b')\, db \,. \tag{7}$$

Integration is done over all impact parameters which lead to the formation of a given vibrational state v. Using Eq. (1) the detailed cross section becomes

$$\sigma_{re}(E_{trans}, v) = \pi[b^2(v) - b^2(v+1)] \,. \tag{8}$$

This corresponds to the area between two concentric rings with radii $b(v)$ and $b(v+1)$. From the set of Eq. (8) with the assumption $b(v_{max}+1) = 0$ one obtains

$$b(v) = \left[1/\pi \sum_{v'=0}^{v_{max}-v} \sigma_{re}(E_{trans}, v_{max} - v')\right]^{1/2} \,. \tag{9}$$

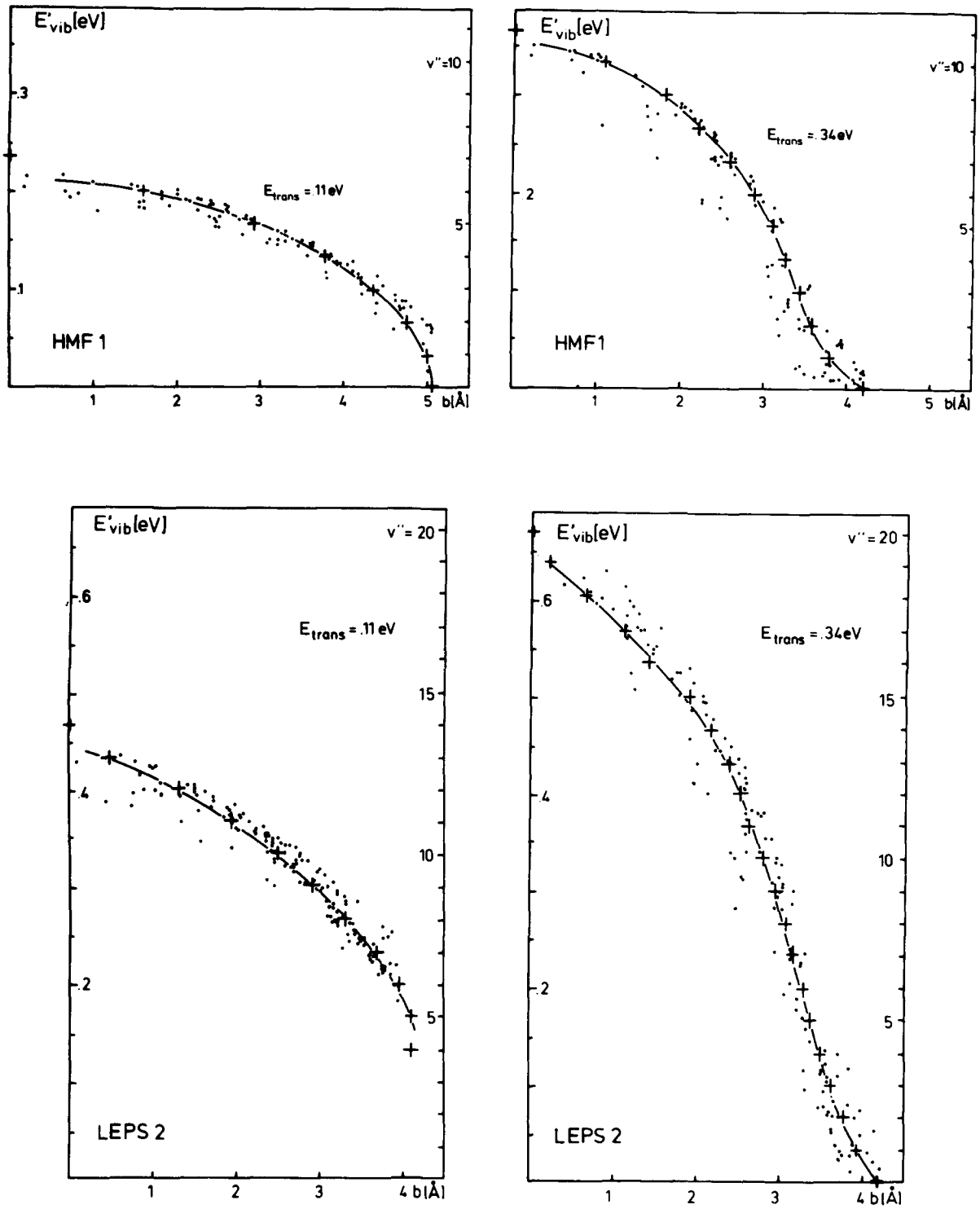

FIG. 14. The function $v(b)$ determined with Eq. (10) for several surfaces in comparison with the results of single trajectories. The calculated values of $v(b)$ are marked as crosses and connected by a line.

This equation can be applied to the results of our trajectory calculations. With the vibrational state population distributions shown in Fig. 8 and the cross sections $\sigma_{re}(E_{\text{trans}})$ determined from the histograms in Fig. 2, one can calculate the cross sections $\sigma_{re}(E_{\text{trans}}, v)$ according to Eq. (6). Then $v(b)$ can be determined from these cross sections by means of Eq. (9). The functions $v(b)$ obtained in this way are shown in Fig. 14 in comparison to the results obtained for single trajectories. The agreement is quite good except for $b=0$ and $b=b_{\max}$ in some cases. These deviations show up because classically not the whole energy intervals are populated in the calculations.

In the same manner the experimental detailed cross sections $\sigma_{re}(E_{\text{trans}}, v)$ (Fig. 13 of Ref. 1), can be immed-

iately converted into $v(b)$. Possibly $v(b)$ is more suitable for a search of correct potential surfaces since few trajectories may suffice for a comparison, while many trajectories have to be calculated to obtain $\sigma_{re}(E_{\text{trans}}, v)$.

ACKNOWLEDGMENT

Financial support by the Deutsche Forschungsgemeinschaft is gratefully acknowledged.

[1]A. Siegel and A. Schultz, J. Chem. Phys. **72**, 6227 (1980).

[2]D. R. Herschbach, "Molecular Beams," in *Advances in Chemical Physics* (Interscience, New York, 1966), Vol. X.

[3]N. H. Hijazi and J. C. Polanyi, J. Chem. Phys. **63**, 2249 (1975).

[4]N. H. Hijazi and J. C. Polanyi, Chem. Phys. **11**, 1 (1975).

[5]H. Eyring and S. H. Lin, "Potential Energy Surfaces," in *Physical Chemistry: An Advanced Treatise*, edited by W. Jost (Academic, New York, 1974), Vol. 6A.

[6]D. L. Bunker, Methods Comput. Physics **10**, 287 (1971).

[7]D. L. Bunker and Ch. A. Parr, J. Chem. Phys. **52**, 5700 (1970).

[8]J. E. Mosch, S. A. Safron, and J. P. Toennies, Chem. Phys. Lett. **29**, 7 (1974).